applied sciences

MDPI

Article

Bearing Crack Diagnosis Using a Smooth Sliding Digital Twin to Overcome Fluctuations Arising in Unknown Conditions

Farzin Piltan [1], Cheol-Hong Kim [2] and Jong-Myon Kim [1,3,*]

[1] Department of Electrical, Electronics and Computer Engineering, University of Ulsan, Ulsan 44610, Korea; piltanfarzin@gmail.com
[2] School of Computer Science and Engineering, Soongsil University, Seoul 06978, Korea; cheolhong@ssu.ac.kr
[3] PD Technology Cooperation, Ulsan 44610, Korea
* Correspondence: jmkim07@ulsan.ac.kr; Tel.: +82-52-259-2217

Abstract: Bearings cause the most breakdowns in induction motors, which can result in significant economic losses. If faults in the bearings are not detected in time, they can cause the whole system to fail. System failures can lead to unexpected breakdowns, threats to worker safety, and huge economic losses. In this investigation, a new approach is proposed for fault diagnosis of bearings under variable low-speed conditions using a smooth sliding digital twin analysis of indirect acoustic emission (AE) signals. The proposed smooth sliding digital twin is designed based on the combination of the proposed autoregressive fuzzy Gauss–Laguerre bearing modeling approach and the proposed smooth sliding fuzzy observer. The proposed approach has four steps. The AE signals are resampled and the root mean square (RMS) feature is extracted from the AE signal in the first step. To estimate the resampled RMS bearing signal, a new smooth sliding digital twin is proposed in the second step. After that, the resampled RMS bearing residual signal is generated using the difference between the original and estimated signals. Next, a support vector machine (SVM) is proposed for crack detection and crack size identification. The effectiveness of this new approach is evaluated by AE signals provided by our lab's bearing dataset, where the benchmark dataset consists of one normal and seven abnormal conditions: ball, outer, inner, outer-ball, inner-ball, inner-outer, and inner-outer-ball. The results demonstrated that the average accuracies of the anomaly diagnosis and crack size identification of AE signals for the bearings used in this new smooth sliding digital twin are 97.75% and 97.78%, respectively.

Keywords: induction motor; bearing; acoustic emission signal; smooth sliding digital twin; autoregressive fuzzy Gauss–Laguerre; fuzzy logic technique; support vector machine; crack detection; crack size identification

Citation: Piltan, F.; Kim, C.-H.; Kim, J.-M. Bearing Crack Diagnosis Using a Smooth Sliding Digital Twin to Overcome Fluctuations Arising in Unknown Conditions. *Appl. Sci.* **2022**, *12*, 6770. https://doi.org/10.3390/app12136770

Academic Editors: Tomasz Figlus and Junfeng Wang

Received: 12 June 2022
Accepted: 1 July 2022
Published: 4 July 2022

1. Introduction

One of the most widely applicable human inventions is the bearing, which prevents wear and tear when moving heavy objects and decreases the friction between moving parts. By using bearings, instead of causing wear and tear, objects can rotate together. Without bearings, the equipment used to rotate needs to be replaced often. Bearings are used in diverse industrial applications, such as power generators, oil refining, machine tool operations, natural gas transportation, and centrifugal/turbocharged pumps. Due to the widespread use of bearings, the probability of defects in these parts is not small. Fault diagnosis in industrial components such as bearings is very useful and valuable. Accurate fault diagnosis can increase safety, extend the lifetime of machinery, and reduce consumption costs. Inner race, outer race, ball race, and cage faults are among the crucial types of bearing anomalies [1,2]. Different sensors, such as vibration, stator current, shaft voltage, and acoustic emission (AE) sensors, can be used to extract the data for the bearings and check their health. In recent years, vibration and AE sensors have found many applications in industry [3].

To design bearing fault diagnosis techniques, various approaches have been carried out that can be used in three main domains: the time domain, frequency domain, and time–frequency domain. Time and frequency domain analyses have the challenge of high feature dimensions. Time–frequency domain analysis, such as the short-time Fourier transform [4], Wigner Ville distribution [5], and wavelet packet transform [6], have been recommended to solve problems associated with the nonstationary and nonlinear nature of the bearings' signals. Moreover, digital twins are an efficient technique for anomaly diagnosis in various applications. These approaches allow for diverse and much more precise analyses by designing models/estimates of the original system [7]. In addition, various techniques can be introduced to design digital twins, such as model-based techniques, signal-based approaches, artificial intelligence–based algorithms, and hybrid schemes [8]. In signal-based approaches, signal processing algorithms can be used for anomaly diagnosis [8,9]. The application of a signal-based algorithm for anomaly detection and identification was suggested in [10]. The application of artificial intelligence–based approaches for anomaly identification was proposed in [9]. These techniques have been used in several applications, such as bearing fault diagnosis and pipeline crack diagnosis [9]. In model-based approaches, mathematical-based fault modeling algorithms can be used for reliable and stable fault detection and identification. In reliable model-based fault diagnosis, the faults are identified using a small dataset; however, mathematical modeling of complex systems is challenging work [11]. Hybrid approaches can be designed based on a combination of the above techniques [12]. These techniques are able to reduce the weakness of each of the above methods and increase their strengths.

Various researchers have implemented rigorous studies in the field of fault diagnosis for bearings using model-based approaches. Model-based approaches for fault diagnosis utilize signal estimation techniques, system identification approaches, and output observation schemes. Allal et al. [13] obtained the residual signals that were calculated based on the difference between original and estimated ones for fault diagnosis using a model-based approach. Although this approach is stable and reliable, there are significant challenges related to signal modeling. Mathematical modeling and identification techniques are the most important methods for signal/system modeling. Although mathematical-based modeling has advantages such as reliability and accuracy, it is difficult to use this method to model nonlinear and complex signals/systems. On the other hand, an identification-based approach is able to model the dynamic behavior of the system by analyzing data extracted from the sensors. Regression-based approaches, such as the autoregressive technique [14] and autoregressive with external input [15], are the most important schemes for identification-based modeling. To improve the robustness of regression-based approaches, the Laguerre filter technique was suggested in [16]. The application of a fuzzy technique to a regression-based identification technique was introduced in [17]. One of the important schemes for model-based fault diagnosis is observation-based approaches. These techniques can be designed by various algorithms, which are categorized into two groups: linear-based observation algorithms and nonlinear-based observation techniques. The proportional-integral observer, proportional-multi-integral observer, and proportional-integral-derivative observer each fall into the group of linear observers. For example, TayebiHaghighi and Koo [18] introduced a proportional-integral (PI) observer for bearing fault diagnosis. To develop the performance of the PI observer, the proportional-multi-integral (PMI) observer for fault diagnosis of bearings was introduced in [19]. Apart from the advantages of linear observers, such as their simplicity of implementation, these methods suffer from a lack of robustness and accuracy in fault modeling. Nonlinear observation approaches have been proposed to overcome the problems of linear observation techniques. Various observers can be listed in the group of nonlinear observers, such as linearized feedback methods, backstepping approaches, Lyapunov algorithms, variable structure schemes, fuzzy methods, and neural network algorithms. For instance, linearized feedback has been applied for accurate fault modeling in [11]. In [20], the vibration signals were modeled by mathematical techniques, and the fault signal was estimated by a feedback

linearization observer. This technique has two significant challenges: stability and system modeling using a mathematical approach. Variable structure algorithms and Lyapunov methods are two influential, robust, nonlinear algorithms [21]. These two algorithms have been used in diverse applications for fault diagnosis in bearings, robotics, and pipelines. High-frequency fluctuations in unknown conditions are a significant challenge of variable structure observers. To reduce the effect of high-frequency fluctuations, various techniques have been suggested, including the super-twisting technique [22], saturation algorithm [23], and high-order variable structure [24].

In this research article, a robust smooth sliding digital twin is recommended for bearing anomaly identification. This method consists of three main parts. First, the AE bearing signals are resampled and the RMS feature is extracted from them. Next, the robust smooth sliding digital twin is designed for modeling and to estimate the RMS feature. After that, the SVM technique is used for feature classification and crack size identification. The main part of this research is the digital twin design. So, to design the proposed digital twin, the indirect (feature) signals are modeled using the proposed autoregressive fuzzy Gauss–Laguerre algorithm. After modeling the feature signal, the indirect observer based on the proposed online tuning sliding fuzzy (smooth sliding) algorithm is designed. The main contributions of the proposed robust smooth sliding digital twin are introduced as:

1. Propose an indirect (RMS feature) AE bearing signal modeling technique using a robust autoregressive fuzzy Gauss–Laguerre algorithm.
2. Design a robust smooth sliding digital twin using the combination of indirect AE bearing signal modeling and an online tuning sliding fuzzy (smooth sliding) algorithm.
3. Apply a machine learning technique to the robust smooth sliding digital twin for feature classification and crack size identification.

This research article has the following sections. In the Section 2, the experimental dataset is explained. The proposed robust smooth sliding digital twin is designed and analyzed in the Section 3. In the Section 4, the results and discussion of the fault diagnosis for bearings are explained. Finally, our conclusions and future work are described in the Section 5.

2. Experimental Dataset

The block diagram of the bearing fault simulator is demonstrated in Figure 1. Based on this figure, this fault simulator has three main parts: a three-phase induction motor, a gearbox, and acoustic emission sensors. To transfer the load to the shaft, a gearbox is used. The acoustic emission sensors are used to collect the bearing data. Based on this figure, a FAG NJ206-E-TVP2 bearing is attached in the shaft. Moreover, a wideband frequency AE sensor (PAC WSα) was used to acquire data when placed on the top of nondrive end shaft bearing at a 21.48 mm displacement under normal and abnormal conditions when the sampling rate is 250 kHz [9]. To simulate the faulty conditions, a bearing with 3-mm and 6-mm crack sizes in length and 0.3-mm crack size in depth and 0.35 mm in width is used [25–27]. Figure 2 shows our lab's testbed, which was used to collect bearing data in normal (NS) and seven abnormal conditions. Moreover, Table 1 shows information about the AE sensors used for data collection [25–27]. Figure 3 illustrates the seven abnormal conditions in the bearing, including ball (BS), inner (IS), outer (OS), inner-ball (IBS), outer-ball (OBS), inner-outer (IOS), and inner-outer-ball (IOBS).

The ball faults are the anomalies found on the balls, the outer faults are the faults found on the outside of the balls, and the inner faults are the faults found on the inside of the balls. Moreover, the other faults are the combination of ball, inner, and outer faults. Furthermore, because fault diagnosis on a low-speed motor is difficult, we considered motor rotation speeds of 300, 400, 450, and 500 RPM. The information of the bearing dataset, comprising the working conditions, motor speed, and crack size of the bearings, is illustrated in Table 2.

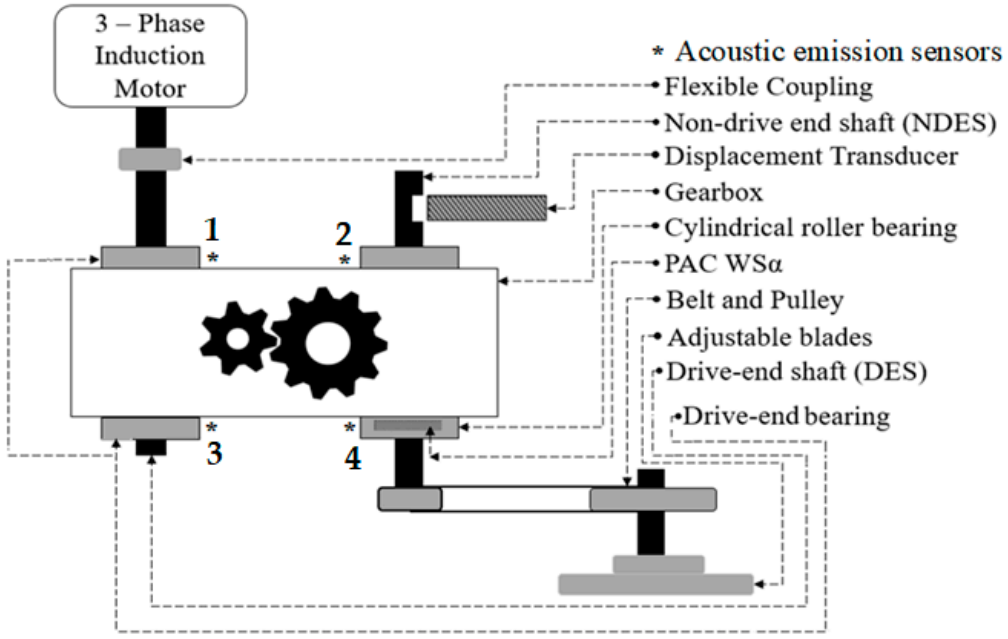

Figure 1. Bearing fault simulator.

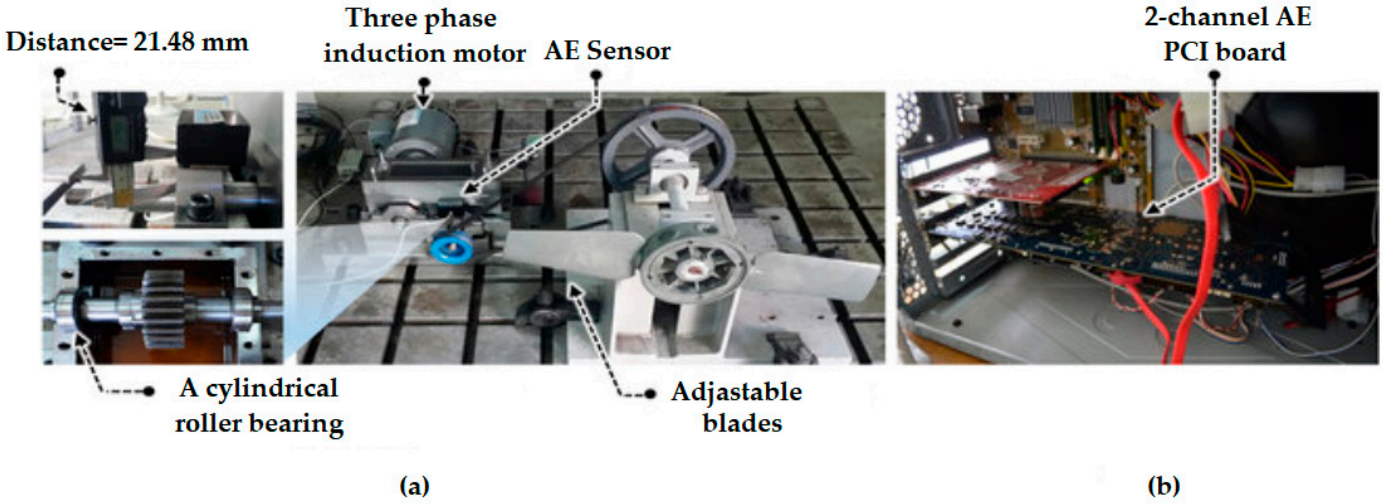

Figure 2. Experimental test for data collection in bearings: (**a**) data generation and (**b**) two-channel acoustic emission PCI board for data acquisition.

Table 1. Sensor and data collection system information [9].

AE Sensor (PAC WSα) Information	PCI Board with Two-Channel AE Sensor Information
Peak sensitivity [V/µbar]: −62 dB Operational frequency range: 100–900 kHz Directionality: ±1.5 dB Resonant frequency: 650 kHz	A/D conversion: 18-bit 40 MHz AE sensor: 2 channels (one has a 10 M samples/s rate, and the other has a 5 M samples/s rate; the two channels are used simultaneously)

(**a**) (**b**) (**c**) (**d**) (**e**) (**f**) (**g**)

Figure 3. Seven abnormal conditions in the bearings: (**a**) OS, (**b**) IS, (**c**) BS, (**d**) IOS, (**e**) IBS, (**f**) OBS, and (**g**) IOBS.

Table 2. Signal information for eight conditions.

Conditions	Speed of Motor [RPM]	Size of Crack [mm]
NS	300, 400, 450, 500	-
OS, IS, BS, IOS, IBS, OBS, IOBS	300, 400, 450, 500	3; 6

3. Proposed Scheme

The proposed scheme for bearing anomaly identification and crack size detection in bearings using a robust smooth sliding digital twin is shown in Figure 4. Bearing anomaly identification and crack size detection using the proposed digital-twin-based algorithm consists of three parts: (a) resampling and featuring, (b) designing the robust smooth sliding digital twin, and (c) bearing anomaly identification and crack size detection using SVM. In the first step, the AE signals extracted from the bearing are resampled and its RMS characteristic is extracted. The second part is the main section of this research. At this stage, the proposed robust smooth sliding digital twin is designed. This part consists of two main sub-sections: modeling and estimation. The first sub-section focuses on modeling the indirect AE bearing (resampled RMS feature) signals using the N. The proposed autoregressive fuzzy Gauss–Laguerre algorithm for normal feature signal modeling is designed using a combination of the autoregressive algorithm, Gaussian methods to improve the power of nonlinearity modeling, a Laguerre filter to overcome the uncertain conditions, and a fuzzy algorithm to modify the power of nonlinearity signal modeling. After modeling the normal resampled RMS signal using the proposed autoregressive fuzzy Gauss–Laguerre algorithm, the signal estimation algorithm is designed using the proposed robust smooth sliding digital twin. The proposed robust smooth sliding digital twin is designed based on the combination of the proposed autoregressive fuzzy Gaussian–Laguerre algorithm for signal modeling, a high-order sliding mode technique to improve the robustness, and a fuzzy approach to overcome fluctuations arising in unknown conditions. After modeling and estimation of the AE feature signals using the robust smooth sliding digital twin, in the Section 3, the residual signals are generated and the SVM technique is used for bearing anomaly identification and crack size detection.

3.1. Resampling and Featuring

To design the proposed indirect robust smooth sliding digital twin, in the initial step, the root mean square (RMS) feature is extracted from the original AE signals according to the following definition.

$$S_{AE}(k)_{rms} = \sqrt{\frac{1}{K}\sum_{i=1}^{K}\left(S_{AE}(k)\right)^2} \quad (1)$$

where $S_{AE}(k)_{rms}$ is a resampled RMS value of the original AE signals in all conditions and K is the number of windows for resampling the original AE signals. The number of samples for NS for all motor speeds (300 RPM, 400 RPM, 450 RPM, and 500 RPM) is 5,000,000. Moreover, the number of samples for OS, IS, BS, IOS, IBS, OBS, and IOBS for all motor

speeds (300 RPM, 400 RPM, 450 RPM, and 500 RPM) and two crack sizes (3 mm and 6 mm) is 7,000,000.

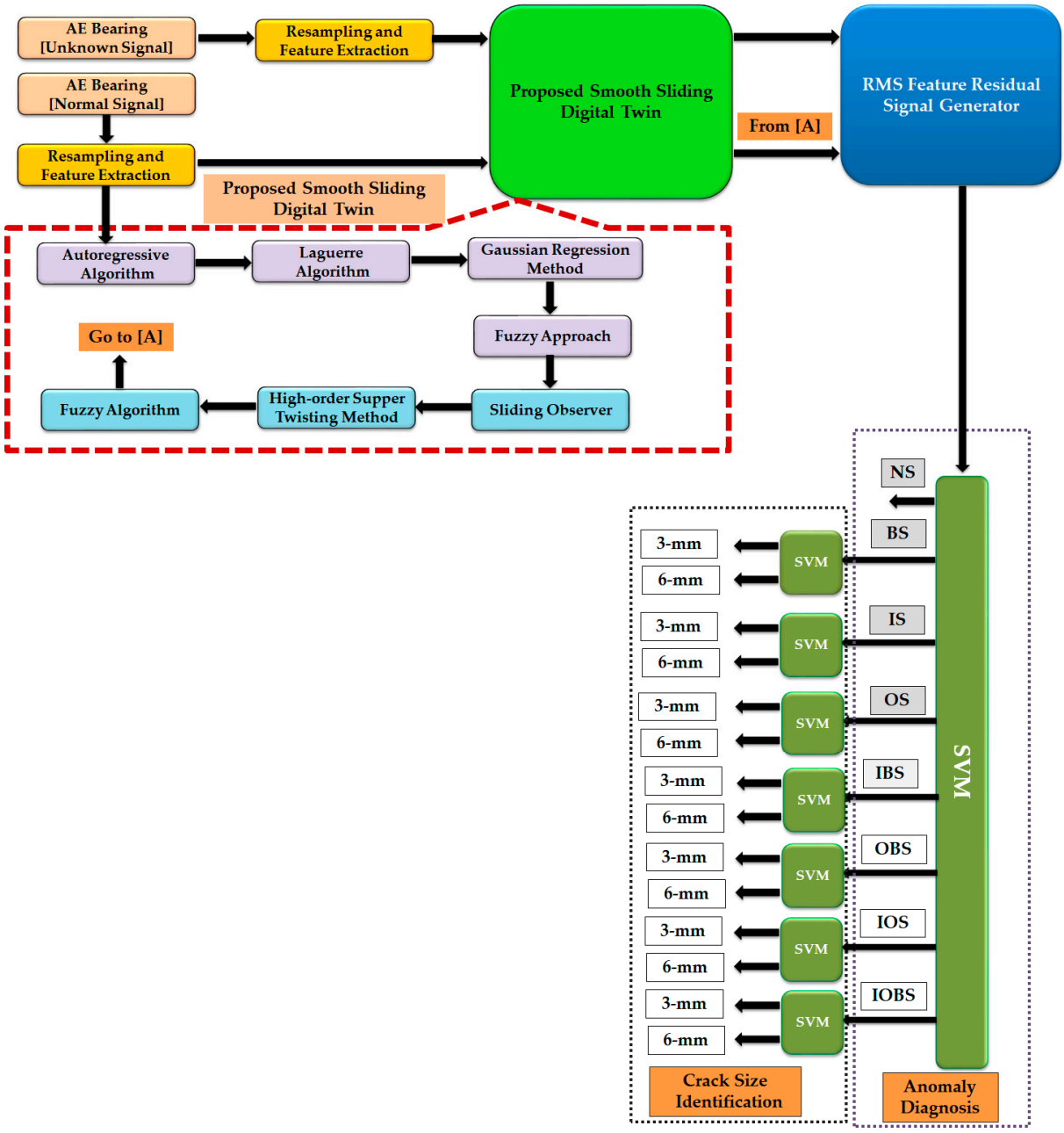

Figure 4. Structure of the proposed robust smooth sliding digital twin with machine learning for anomaly diagnosis and crack size identification.

The original AE signal was divided into 6000 windows, and each 12,500 samples is defined as a window. Next, we obtained the RMS feature for each window. After resampling and extracting the RMS feature from the original AE signals of the bearing, the proposed indirect robust smooth sliding digital twin is designed.

3.2. Proposed Robust Smooth Sliding Digital Twin

According to Figure 4, after resampling and RMS feature extraction from the original AE signals of the bearing, the proposed indirect robust smooth sliding digital twin is designed based on the following steps. To design the proposed scheme, we have two main steps: (a) feature modeling using the proposed autoregressive fuzzy Gauss–Laguerre

algorithm and (b) feature estimation using the combination of an autoregressive fuzzy Gauss–Laguerre modeling algorithm and the proposed high-order sliding fuzzy observer.

3.2.1. Proposed Autoregressive Fuzzy Gauss–Laguerre Feature Modeling

Based on Figure 4, to design an indirect robust smooth sliding digital twin, feature modeling is the first step. Thus, the proposed autoregressive fuzzy Gauss–Laguerre algorithm is designed to model the known (normal feature signal when the speed of the motor is 300 RPM) RMS feature signal. The proposed autoregressive fuzzy Gauss–Laguerre algorithm is designed using the combination of the following techniques: (a) an autoregressive algorithm, (b) Gaussian methods to improve the power of nonlinearity modeling, (c) a Laguerre filter to overcome the uncertain conditions, and (d) a fuzzy algorithm to modify the power of nonlinearity signal modeling. The autoregressive algorithm in introduced using the following definition.

$$\begin{cases} \varnothing_a(k+1) = [C_\varnothing \varnothing_a(k) + C_i \mathrm{S}_i(k)] + e_a(k) + U(k) \\ \varepsilon_a(k) = (C_o)^T \varnothing_a(k) \end{cases} \tag{2}$$

where $\varnothing_a(k)$ is the state of RMS feature modeling using the autoregressive algorithm, $\mathrm{S}_i(k)$ is the RMS feature from the original AE signals of the bearing, $e_a(k)$ is the autoregressive error for modeling the RMS feature signal, $U(k)$ is the unknown/uncertain state for RMS feature modeling, $\varepsilon_a(k)$ is the output function of RMS feature signal modeling using the autoregressive technique, and $(C_\varnothing, C_i, C_o)$ are coefficients (the state of RMS feature modeling, RMS feature from the original AE signals of bearing, and output function of RMS feature signal modeling) of signal modeling. Furthermore, the error of autoregressive RMS feature signal modeling is calculated from the following equation.

$$e_a(k) = \varepsilon_a(k) - \varepsilon_a(k-1) \tag{3}$$

To reduce the error of RMS feature signal modeling using the autoregressive technique, nonlinear-based signal modeling can be very useful. Thus, the Gaussian method is suggested to enhance the power of nonlinearity modeling. The autoregressive Gaussian algorithm is introduced using the following definition.

$$\begin{cases} \varnothing_{ag}(k+1) = \left[C_\varnothing \varnothing_{ag}(k) + C_i \mathrm{S}_i(k)\right] + e_{ag}(k) + U(k) \\ \varepsilon_{ag}(k) = (C_o)^T {\chi_\mathrm{g}}^{-1} \varnothing_{ag}(k) \end{cases} \tag{4}$$

where $\varnothing_{ag}(k)$ is the state of RMS feature modeling using the autoregressive Gaussian algorithm, $e_{ag}(k)$ is the error of the autoregressive Gaussian for modeling the RMS feature signal g, $\varepsilon_{ag}(k)$ is the output function of RMS feature signal modeling using the autoregressive Gaussian technique, and χ_g is the covariance matrix for RMS feature modeling using the Gaussian algorithm. Furthermore, the covariance matrix (χ_g) for RMS feature modeling in known conditions using the Gaussian algorithm is represented as follows.

$$\chi_\mathrm{g} = \omega^2 e^{\left(-0.5 {\varnothing_{ag}}^T B^{-1} \varnothing_{ag}\right)} + V \tag{5}$$

$$B = diag(N)^2 \tag{6}$$

where ω is the variance of the RMS feature of the AE signal in known conditions, V is the noise variance, and N is the kernel width. Additionally, the error of autoregressive Gaussian RMS feature signal modeling is considered from the following equation.

$$e_{ag}(k) = \varepsilon_{ag}(k) - \varepsilon_{ag}(k-1) \tag{7}$$

The next challenge of RMS feature (indirect) AE signal modeling is the robustness. To increase the robustness of RMS feature signal modeling and reduce the error of RMS feature signal modeling using the autoregressive Gaussian technique, the Laguerre filter technique is combined with the autoregressive Gaussian algorithm. The autoregressive Gauss–Laguerre procedure is defined using the following description.

$$\begin{cases} \varnothing_{ag-l}(k+1) = \left[C_{\varnothing}\varnothing_{ag-l}(k) + C_i S_i(k) + C_{\varepsilon}\varepsilon_{ag-l}(k)\right] + e_{ag-l}(k) + U(k) \\ \varepsilon_{ag-l}(k) = (C_o)^T \chi_g{}^{-1}\varnothing_{ag-l}(k) \end{cases} \tag{8}$$

At this point, $\varnothing_{ag-l}(k)$ is the state of RMS feature modeling using the autoregressive Gauss–Laguerre algorithm, $e_{ag-l}(k)$ is the error of the autoregressive Gauss–Laguerre for modeling the RMS feature signal, $\varepsilon_{ag-l}(k)$ is the output function of RMS feature signal modeling using the autoregressive Gauss–Laguerre technique, and C_{ε} is the coefficient for RMS feature modeling using the autoregressive Gauss–Laguerre algorithm. In addition, the error of autoregressive Gauss–Laguerre RMS feature signal modeling is considered from the following definition.

$$e_{ag-l}(k) = \varepsilon_{ag-l}(k) - \varepsilon_{ag-l}(k-1) \tag{9}$$

Finally, to modify the power of nonlinearity signal modeling for the application of the fuzzy algorithm in the autoregressive Gauss–Laguerre to modeling, the RMS feature signal is announced. The autoregressive fuzzy Gauss–Laguerre method is defined using the following explanation.

$$\begin{cases} \varnothing_{afg-l}(k+1) = \left[C_{\varnothing}\varnothing_{afg-l}(k) + C_i S_i(k) + C_{\varepsilon}\varepsilon_{afg-l}(k)\right] + e_{afg-l}(k) + U(k) + C_{\mathrm{f}} f(k) \\ \varepsilon_{afg-l}(k) = (C_o)^T \chi_g{}^{-1}\varnothing_{afg-l}(k) \end{cases} \tag{10}$$

Currently, $\varnothing_{afg-l}(k)$ is the state of RMS feature modeling using the autoregressive fuzzy Gauss–Laguerre algorithm, $e_{afg-l}(k)$ is the error of the autoregressive fuzzy Gauss–Laguerre for modeling the RMS feature signal, $\varepsilon_{afg-l}(k)$ is the output function of RMS feature signal modeling using the autoregressive fuzzy Gauss–Laguerre technique, $f(k)$ is the fuzzy function used to improve the power of uncertain signal modeling, and C_{f} is the coefficient for RMS feature modeling using the autoregressive fuzzy Gauss–Laguerre algorithm. Furthermore, the error of autoregressive fuzzy Gauss–Laguerre RMS feature signal modeling is considered from the subsequent description.

$$e_{afg-l}(k) = \varepsilon_{afg-l}(k) - \varepsilon_{afg-l}(k-1) \tag{11}$$

Algorithm 1 shows the steps to designing the proposed RMS feature modeling using the autoregressive fuzzy Gauss–Laguerre approach.

3.2.2. Proposed Higher-Order Sliding Fuzzy Observer

After modeling the known RMS feature signal using the proposed autoregressive fuzzy Gauss–Laguerre approach, an observation algorithm based on the proposed higher-order sliding fuzzy technique is designed in the second step. The proposed observer is used to estimate the RMS signal of the bearing in all conditions. To design a proposed observer, a sliding observation algorithm is first suggested. Using a sliding observer is a nonlinear and robust technique to estimate the signals. To improve the robustness of the classical (second-order) sliding observer, a higher-order technique is suggested in this work. Apart from the robustness of the high-order sliding observer, this technique suffers from high-frequency oscillation (chattering phenomenon). To reduce the effect of chattering in the high-order sliding observer, a fuzzy algorithm is suggested. A high-order sliding fuzzy

observer can be used to overcome fluctuations arising in uncertain/unknown conditions. First, the combination of the proposed autoregressive fuzzy Gauss–Laguerre RMS signal modeling approach and second-order sliding observer is introduced as follows.

$$\begin{cases} \varnothing_{(afg-l)-s}(k+1) = \left[C_{\varnothing}\varnothing_{(afg-l)-s}(k) + C_i S_i(k) + C_{\varepsilon}\varepsilon_{(afg-l)-s}(k)\right] \\ \quad + e_{afg-l}(k) + U_{(afg-l)-s}(k) + C_f f(k) + C_{u(s)} sgn U_{(afg-l)-s}(k) \\ \\ \varepsilon_{(afg-l)-s}(k) = (C_o)^T {\chi_g}^{-1} \varnothing_{(afg-l)-s}(k) \end{cases} \tag{12}$$

Algorithm 1: Proposed RMS feature modeling using the autoregressive fuzzy Gauss–Laguerre approach.

1:	RMS feature signal modeling using the autoregressive procedure; Equation (2)
	Detail
1.1	Calculate $e_a(k) \leftarrow \varepsilon_a(k) - \varepsilon_a(k-1)$, Equation (3)
1.2	Calculate $\varnothing_a(k+1) \leftarrow [C_{\varnothing}\varnothing_a(k) + C_i S_i(k)] + e_a(k) + U(k)$, Equation (2)
1.3	Calculate $\varepsilon_a(k) \leftarrow (C_o)^T \varnothing_a(k)$, Equation (2)
2:	Gaussian method is applied to the autoregressive approach to enhance the power of nonlinearity modeling; Equation (4)
	Detail
2.1	Calculate $e_{ag}(k) \leftarrow \varepsilon_{ag}(k) - \varepsilon_{ag}(k-1)$, Equation (7)
2.2	Calculate $\varnothing_{ag}(k+1) \leftarrow \left[C_{\varnothing}\varnothing_{ag}(k) + C_i S_i(k)\right] + e_{ag}(k) + U(k)$, Equation (4)
2.3	Calculate $\chi_g \leftarrow \omega^2 e^{(-0.5\varnothing_{ag}{}^T B^{-1}\varnothing_{ag})} + V$, Equation (5)
2.4	Calculate $B \leftarrow diag(N)^2$, Equation (5)
2.5	Calculate $\varepsilon_{ag}(k) \leftarrow (C_o)^T {\chi_g}^{-1}\varnothing_{ag}(k)$, Equation (4)
3:	Increase the robustness of RMS feature signal modeling and reduce the error of RMS feature signal modeling using the combination of the Laguerre filter technique and autoregressive Gaussian algorithm; Equation (8)
	Detail
3.1	Calculate $e_{ag-l}(k) \leftarrow \varepsilon_{ag-l}(k) - \varepsilon_{ag-l}(k-1)$, Equation (9)
3.2	Calculate $\varnothing_{ag-l}(k+1) \leftarrow \left[C_{\varnothing}\varnothing_{ag-l}(k) + C_i S_i(k) + C_{\varepsilon}\varepsilon_{ag-l}(k)\right] + e_{ag-l}(k) + U(k)$, Equation (8)
3.3	Calculate $\varepsilon_{ag-l}(k) \leftarrow (C_o)^T {\chi_g}^{-1}\varnothing_{ag-l}(k)$, Equation (8)
4:	To modify the power of nonlinearity signal modeling, the application of a fuzzy algorithm in the autoregressive Gauss–Laguerre is announced; Equation (10)
	Detail
4.1	Calculate $e_{afg-l}(k) \leftarrow \varepsilon_{afg-l}(k) - \varepsilon_{afg-l}(k-1)$, Equation (11)
4.2	Calculate $\varnothing_{afg-l}(k+1) \leftarrow \left[C_{\varnothing}\varnothing_{afg-l}(k) + C_i S_i(k) + C_{\varepsilon}\varepsilon_{afg-l}(k)\right] + e_{afg-l}(k) + U(k) + C_f f(k)$, Equation (10)
4.3	Calculate $\varepsilon_{afg-l}(k) = (C_o)^T {\chi_g}^{-1}\varnothing_{afg-l}(k)$, Equation (10)

Currently, $\varnothing_{(afg-l)-s}(k)$ is the state of RMS feature estimation using the combination of the autoregressive fuzzy Gauss–Laguerre algorithm and second-order sliding observer, $U_{(afg-l)-s}(k)$ is the uncertainty estimation using the combination of the autoregressive fuzzy Gauss–Laguerre algorithm and second-order sliding observer, $\varepsilon_{(afg-l)-s}(k)$ is the output function of RMS feature signal estimation using the combination of the autoregressive fuzzy Gauss–Laguerre algorithm and second-order sliding observer, and $C_{u(s)}$ is the coefficient of the second-order sliding observer for RMS feature estimation using the combination of the autoregressive fuzzy Gauss–Laguerre algorithm and second-order sliding observer. Moreover, the uncertainties using the combination of the autoregressive

fuzzy Gauss–Laguerre algorithm and second-order sliding observer are described using the following explanation.

$$U_{(afg-l)-s}(k) = C_{\mathrm{u(s1)}}\left(\mathrm{S}_i(k) - \varepsilon_{(afg-l)-s}(k)\right) + C_{\mathrm{u(s2)}}sgn\left(\mathrm{S}_i(k) - \varepsilon_{(afg-l)-s}(k)\right) \quad (13)$$

where $\left(C_{\mathrm{u(s1)}}\right.$ and $\left.C_{\mathrm{u(s2)}}\right)$ are the coefficients of uncertain estimation using the combination of the autoregressive fuzzy Gauss–Laguerre algorithm and second-order sliding observer. To recover the robustness in the classical sliding observer, the higher-order technique is recommended in this effort. The definition of the high-order sliding observer is introduced using the following explanation.

$$\lambda(k) = C_\alpha \| \left(\mathrm{S}_i(k) - \varepsilon_{(afg-l)-s}(k)\right) \|^{0.5} + C_\beta sgn\left(\mathrm{S}_i(k) - \varepsilon_{(afg-l)-s}(k)\right) \quad (14)$$

where $\lambda(k)$ is the high-order definition for the sliding observer and (C_α and C_β) are the coefficients for RMS signal estimation in the high-order sliding observer. In the presence of uncertain conditions, the estimation error increases. The twisted algorithm is used to reduce the error of estimation in uncertain conditions. Based on the high-order technique, the twisted algorithm is introduced as follows.

$$\begin{cases} \Gamma(k) = -(C_\alpha \| \left(\mathrm{S}_i(k) - \varepsilon_{(afg-l)-s}(k)\right) \|^{0.5} + C_\beta sgn(\mathrm{S}_i(k) - \varepsilon_{(afg-l)-s}(k))) \\ \dot{\Gamma(k)} = C_\beta sgn\left(\mathrm{S}_i(k) - \varepsilon_{(afg-l)-s}(k)\right) \end{cases} \quad (15)$$

where $\dot{\Gamma(k)}$ is the twisting function. Thus, the combination of the proposed autoregressive fuzzy Gauss–Laguerre RMS signal modeling approach and high-order sliding observer is presented as follows.

$$\begin{cases} \varnothing_{(afg-l)-hs}(k+1) = \left[C_\varnothing \varnothing_{(afg-l)-hs}(k) + C_i \mathrm{S}_i(k) + C_\varepsilon \varepsilon_{(afg-l)-hs}(k)\right] \\ \quad + e_{afg-l}(k) + U_{(afg-l)-hs}(k) + C_\mathrm{f} f(k) + C_{\mathrm{u(s)}} sgn\left|U_{(afg-l)-hs}(k)\right|^{\frac{2}{3}} \\ \\ \varepsilon_{(afg-l)-hs}(k) = (C_o)^T \chi_\mathrm{g}{}^{-1} \varnothing_{(afg-l)-hs}(k) \end{cases} \quad (16)$$

where $\varnothing_{(afg-l)-hs}(k)$ is the state of RMS feature estimation using the combination of the autoregressive fuzzy Gauss–Laguerre algorithm and high-order sliding observer, $U_{(afg-l)-hs}(k)$ is the uncertainty estimation using the combination of the autoregressive fuzzy Gauss–Laguerre algorithm and high-order sliding observer, and $\varepsilon_{(afg-l)-hs}(k)$ is the output function of RMS feature signal estimation using the combination of the autoregressive fuzzy Gauss–Laguerre algorithm and high-order sliding observer. Furthermore, the uncertainties using the combination of the autoregressive fuzzy Gauss–Laguerre algorithm, high-order sliding observer, and twisting algorithm are described using the following explanation.

$$\begin{aligned} U_{(afg-l)-hs}(k) = \; & C_{\mathrm{u(s1)}}\left(\mathrm{S}_i(k) - \varepsilon_{(afg-l)-hs}(k)\right) + C_{\mathrm{u(s2)}} sgn\left(\mathrm{S}_i(k) - \varepsilon_{(afg-l)-hs}(k)\right) \\ & + C_\alpha \| \left(\mathrm{S}_i(k) - \varepsilon_{(afg-l)-s}(k)\right) \|^{0.5} + C_\beta sgn\left(\mathrm{S}_i(k) - \varepsilon_{(afg-l)-s}(k)\right) - \Gamma(k) \end{aligned} \quad (17)$$

To condense the consequence of high-frequency oscillation in the combined autoregressive fuzzy Gauss–Laguerre algorithm and high-order sliding observer, a fuzzy algorithm is recommended. Combining the autoregressive fuzzy Gauss–Laguerre algorithm and high-order sliding fuzzy observer (in the proposed smooth sliding digital twin) can be used

to overcome the fluctuations arising in uncertain/unknown conditions. Consequently, the proposed smooth digital twin is obtainable, as described by the following definition.

$$\begin{cases} \varnothing_{SSDT}(k+1) = [C_{\varnothing}\varnothing_{SSDT}(k) + C_i S_i(k) + C_{\varepsilon}\varepsilon_{SSDT}(k)] \\ +e_{afg-l}(k) + U_{SSDT}(k) + C_f f(k) + C_{u(s)} sgn|U_{SSDT}(k)|^{\frac{2}{3}} \\ \\ \varepsilon_{SSDT}(k) = (C_o)^T \chi_g{}^{-1} \varnothing_{SSDT}(k) \end{cases} \tag{18}$$

where $\varnothing_{SSDT}(k)$ is the state of RMS feature estimation using the proposed smooth sliding digital twin, $U_{SSDT}(k)$ is the uncertainty estimation using the proposed smooth sliding digital twin, and $\varepsilon_{SSDT}(k)$ is the output function of RMS feature signal estimation using the proposed smooth sliding digital twin. Additionally, the uncertainties using the proposed smooth sliding digital twin are described using the following explanation.

$$\begin{aligned} U_{SSDT}(k) = \; & C_{u(s1)}(S_i(k) - \varepsilon_{SSDT}(k)) + C_{u(s2)} sgn(S_i(k) - \varepsilon_{SSDT}(k)) + C_{\alpha}\|(S_i(k) - \varepsilon_{SSDT}(k))\|^{0.5} \\ & + C_{\beta} sgn(S_i(k) - \varepsilon_{SSDT}(k)) + C_f U_f(k) - \Gamma(k) \end{aligned} \tag{19}$$

where $U_f(k)$ is the uncertainty estimation using the fuzzy algorithm, and C_f is the fuzzy coefficient used to reduce the error of the uncertainty estimation and decrease the effect of chattering. The uncertainty estimation using the fuzzy technique is defined using the following definition.

Algorithm 2: Proposed smooth sliding digital twin approach.

1:	RMS signal estimation using the combination of the proposed autoregressive fuzzy Gauss–Laguerre RMS signal modeling approach and second-order sliding observer; Equation (12)
	Detail
1.1	Calculate $U_{(afg-l)-s}(k) \leftarrow C_{u(s1)}\left(S_i(k) - \varepsilon_{(afg-l)-s}(k)\right) + C_{u(s2)} sgn\left(S_i(k) - \varepsilon_{(afg-l)-s}(k)\right)$, Equation (13)
1.2	Calculate $\varnothing_{(afg-l)-s}(k+1) \leftarrow \left[C_{\varnothing}\varnothing_{(afg-l)-s}(k) + C_i S_i(k) + C_{\varepsilon}\varepsilon_{(afg-l)-s}(k)\right] + e_{afg-l}(k)$ $+U_{(afg-l)-s}(k) + C_f f(k) + C_{u(s)} sgn U_{(afg-l)-s}(k)$, Equation (12)
1.3	Calculate $\varepsilon_{(afg-l)-s}(k) \leftarrow (C_o)^T \chi_g{}^{-1} \varnothing_{(afg-l)-s}(k)$, Equation (12)
2:	Improve the robustness of RMS signal estimation using the combination of the proposed autoregressive fuzzy Gauss–Laguerre RMS signal modeling approach and high-order sliding observer; Equation (16)
	Detail
2.1	Calculate $\lambda(k) \leftarrow C_{\alpha}\|\left(S_i(k) - \varepsilon_{(afg-l)-s}(k)\right)\|^{0.5} + C_{\beta} sgn\left(S_i(k) - \varepsilon_{(afg-l)-s}(k)\right)$, Equation (14)
2.2	Calculate $\Gamma(k) \leftarrow -(C_{\alpha}\|\left(S_i(k) - \varepsilon_{(afg-l)-s}(k)\right)\|^{0.5} + C_{\beta} sgn\left(S_i(k) - \varepsilon_{(afg-l)-s}(k)\right))$, Equation (15)
2.3	Calculate $\dot{\Gamma}(k) \leftarrow C_{\beta} sgn\left(S_i(k) - \varepsilon_{(afg-l)-s}(k)\right)$, Equation (15)
2.4	Calculate $U_{(afg-l)-hs}(k) \leftarrow C_{u(s1)}\left(S_i(k) - \varepsilon_{(afg-l)-hs}(k)\right) +$ $C_{u(s2)} sgn\left(S_i(k) - \varepsilon_{(afg-l)-hs}(k)\right) + C_{\alpha}\|\left(S_i(k) - \varepsilon_{(afg-l)-s}(k)\right)\|^{0.5} +$ $C_{\beta} sgn\left(S_i(k) - \varepsilon_{(afg-l)-s}(k)\right) - \Gamma(k)$, Equation (17)
2.5	Calculate $\varnothing_{(afg-l)-hs}(k+1) \leftarrow \left[C_{\varnothing}\varnothing_{(afg-l)-hs}(k) + C_i S_i(k) + C_{\varepsilon}\varepsilon_{(afg-l)-hs}(k)\right]$ $+e_{afg-l}(k) + U_{(afg-l)-hs}(k) + C_f f(k) + C_{u(s)} sgn\left\|U_{(afg-l)-hs}(k)\right\|^{\frac{2}{3}}$, Equation (16)
2.6	Calculate $\varepsilon_{(afg-l)-hs}(k) \leftarrow (C_o)^T \chi_g{}^{-1} \varnothing_{(afg-l)-hs}(k)$, Equation (16)

Algorithm 2: *Cont.*

3:	Reduce the effect of the chattering phenomenon using the combination of the autoregressive fuzzy Gauss–Laguerre algorithm, high-order sliding observer, and fuzzy algorithm to design the proposed smooth sliding digital twin; Equation (18)
	Detail
3.1	Calculate $U_{SSDT}(k) \leftarrow C_{u(s1)}(S_i(k) - \varepsilon_{SSDT}(k)) + C_{u(s2)} sgn(S_i(k) - \varepsilon_{SSDT}(k)) + C_\alpha \|(S_i(k) - \varepsilon_{SSDT}(k))\|^{0.5} + C_\beta sgn(S_i(k) - \varepsilon_{SSDT}(k)) + C_f U_f(k) - \Gamma(k)$, Equation (19)
3.2	Calculate $\varnothing_{SSDT}(k+1) \leftarrow [C_\varnothing \varnothing_{SSDT}(k) + C_i S_i(k) + C_\varepsilon \varepsilon_{SSDT}(k)] + e_{afg-l}(k) + U_{SSDT}(k) + C_f f(k) + C_{u(s)} sgn\|U_{SSDT}(k)\|^{\frac{2}{3}}$, Equation (18)
3.3	Calculate $\varepsilon_{SSDT}(k) = (C_o)^T {\chi_g}^{-1} \varnothing_{SSDT}(k)$, Equation (18)

$$U_f(k) = \frac{\sum_z U_z \times \Theta_z}{\sum_z \Theta_z}, \Theta_z = \sum_z e^{(-0.5 \sum_j (\frac{\phi(k) - \mu_z}{\chi_g})^2)} \quad (20)$$

where $U_z(k)$ is the uncertainty, μ_z is a membership function used to calculate the fuzzy estimation, and χ_g is the covariance matrix. Algorithm 2 shows the steps used to design the proposed smooth sliding digital twin to overcome fluctuations arising in unknown conditions.

3.3. Bearing Anomaly Identification and Crack Size Detection

Based on Figure 4, after resampling and RMS feature extraction from the AE signal of bearing, the RMS signal in known conditions is modeled using the proposed autoregressive fuzzy Gauss–Laguerre algorithm. After that, to estimate the RMS signals in all conditions, the proposed smooth sliding digital twin based on the combination of the proposed autoregressive fuzzy Gauss–Laguerre algorithm and high-order sliding fuzzy observer is designed. In this part, the residual signal is generated based on the difference between the original RMS signal and the estimated RMS signal of the bearing. The residual signal of the proposed robust smooth sliding digital twin, $(r_{SSDT}(k))$, is obtained by the following definition.

$$r_{SSDT}(k) = S_{AE}(k)_{rms} - \varepsilon_{SSDT}(k) \quad (21)$$

After generating the residual signal, SVM is used for bearing anomaly identification and crack size detection [8,9].

4. Experimental Results

To test the effectiveness of the proposed smooth sliding digital twin, the AE bearing dataset is used [9]. Figure 5 illustrates the original AE signals for normal and abnormal states. Based on this figure classification, the normal and abnormal conditions are difficult to observe.

To reduce the complexity for modeling and estimation, the indirect observation algorithm is suggested in this work. To design the indirect observer, the resampled RMS feature is extracted from the original AE signals of the bearing and the RMS signal is modeled and estimated. The original AE signal is divided into 6000 windows (each group of 12,500 samples is defined as a window). Next, we obtained the RMS feature for each window. Figure 6 illustrates the resampled RMS signals for all conditions that were extracted from the original AE signals for the bearing.

In the next step, the resampled RMS signal in known conditions (based on Table 2, using the normal state when the motor speed is 300 RPM) is modeled. To test the power of the indirect AE signal modeling using the proposed autoregressive fuzzy Gauss–Laguerre algorithm, this technique is compared with the autoregressive Gauss–Laguerre technique and autoregressive Gaussian method. Figure 7 illustrates the errors of RMS signal modeling using the proposed autoregressive fuzzy Gauss–Laguerre algorithm, autoregressive Gauss–Laguerre technique, and autoregressive Gaussian method. Based on this figure, the error of the proposed autoregressive fuzzy Gauss–Laguerre algorithm is less than the other two methods.

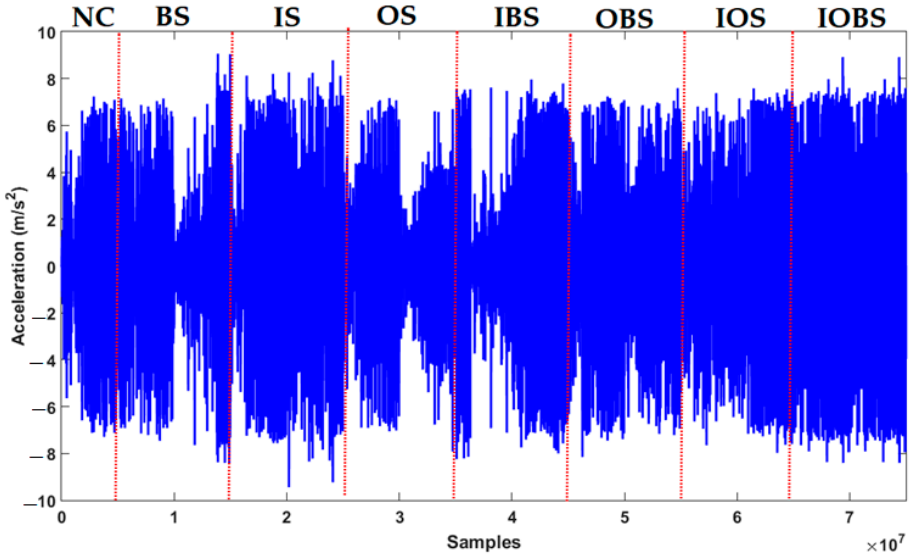

Figure 5. Original AE signals for the bearing.

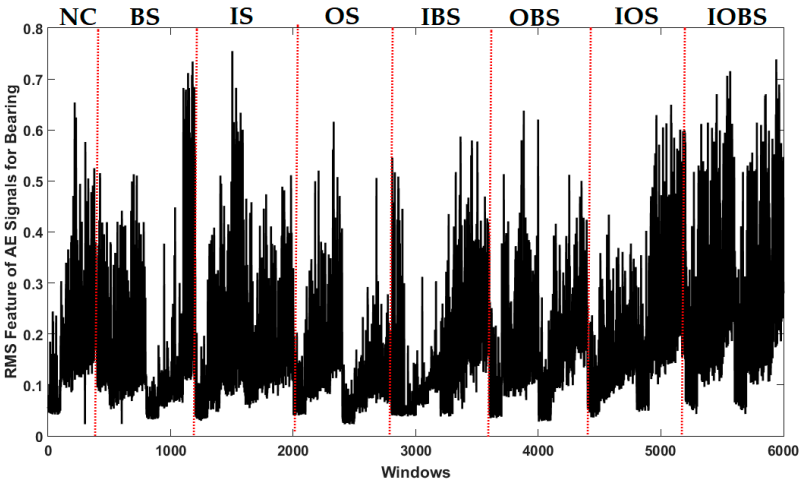

Figure 6. RMS of original AE signals for the bearing.

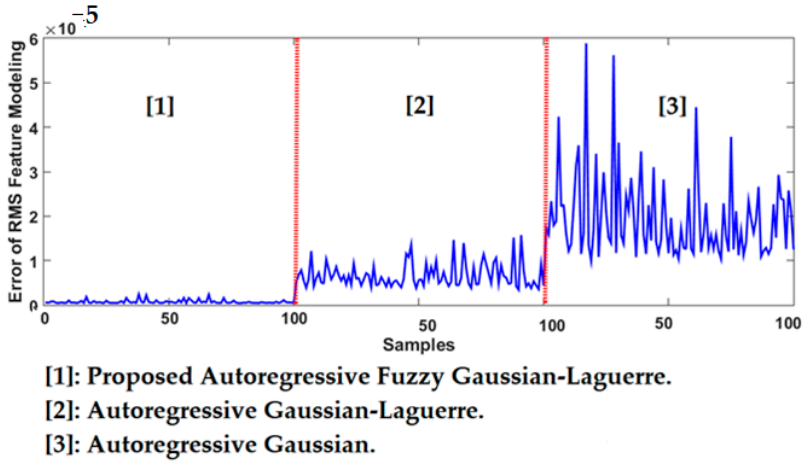

Figure 7. The error of RMS signal modeling using the proposed autoregressive fuzzy Gauss–Laguerre algorithm, autoregressive Gauss–Laguerre technique, and autoregressive Gaussian method for normal conditions.

The other challenges of signal modeling are related to stability and robustness. To test the stability and robustness of the proposed autoregressive fuzzy Gauss–Laguerre algorithm, autoregressive Gauss–Laguerre technique, and autoregressive Gaussian method, the signal modeling errors are checked in normal conditions when the motor speeds are 300 RPM, 400 RPM, 450 RPM, and 500 RPM. Figure 8 illustrates the stability and robustness in the proposed autoregressive fuzzy Gauss–Laguerre algorithm, autoregressive Gauss–Laguerre technique, and autoregressive Gaussian method.

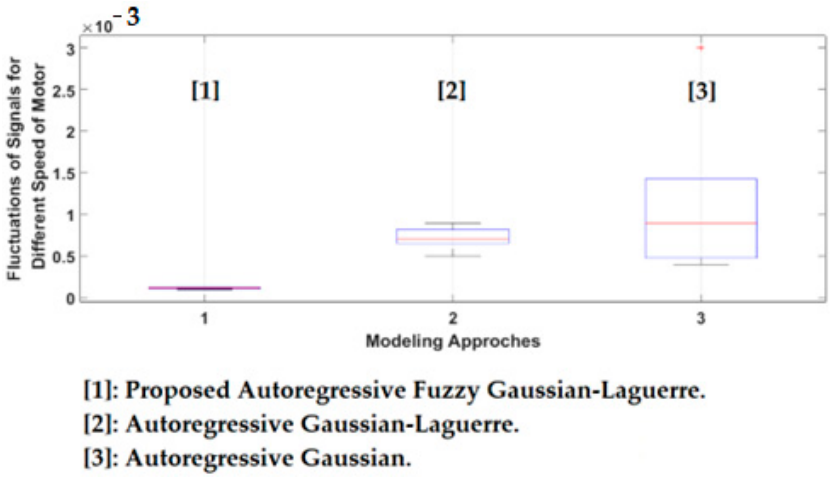

Figure 8. Robustness and stability of RMS signal modeling using the proposed autoregressive fuzzy Gauss–Laguerre algorithm, autoregressive Gauss–Laguerre technique, and autoregressive Gaussian method for normal conditions.

Based on this figure the error of the proposed autoregressive fuzzy Gauss–Laguerre algorithm is less than the other two techniques. Based on Figure 8, the proposed autoregressive fuzzy Gauss–Laguerre algorithm and autoregressive Gauss–Laguerre technique are more robust than the autoregressive Gaussian method. According to the results in Figures 7 and 8, the proposed autoregressive fuzzy Gauss–Laguerre algorithm is suggested for RMS signal modeling. To test the power of RMS (indirect) signal estimation, the proposed smooth sliding digital twin is compared with the high-order sliding digital twin and sliding digital twin. Figure 9 illustrates the residual signals of the proposed smooth sliding digital twin.

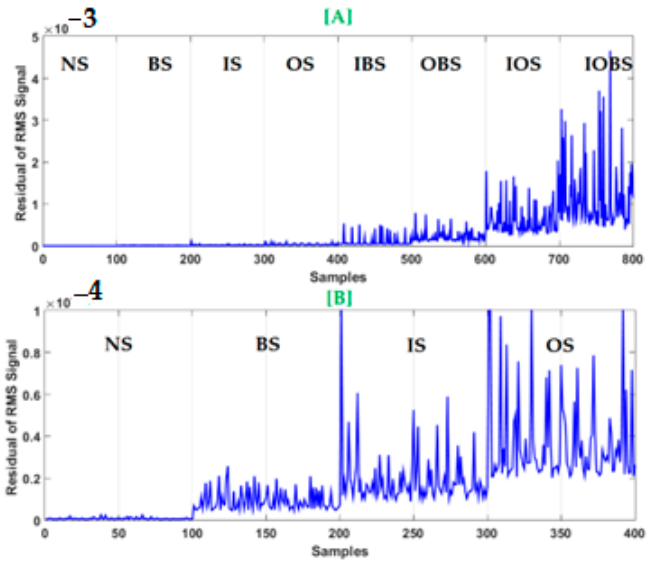

Figure 9. Residual RMS signal using proposed smooth sliding digital twin. (**A**) all conditions, (**B**) zoom view for four conditions.

According to this figure, the difference between signal levels in different classes is much better than in Figure 6. This increases the anomaly detection and identification performance. Based on this figure the level of the residual signal in NS is less than the faulty conditions. Thus, the performance of fault detection in the proposed algorithm is perfect. Furthermore, the difference between residual signals in different anomaly condition is completely different. This makes the quality of the anomaly signal diagnosis excellent in this case. Figures 10 and 11 show the residual of RMS signals in the higher-order sliding digital twin and sliding digital twin, respectively. Based on Figures 10 and 11, the high-frequency oscillation in the high-order sliding digital twin is less than in the sliding digital twin. This means that the high-order technique can reduce the high-frequency oscillation. According to Figure 10, it is difficult to distinguish between OBS and IOS, as well as between NS and IS, using high-order sliding digital twin. In addition, based on Figure 11, the challenging area in sliding digital twin are between NS and IS, between BS and OS, and between IBS and OBS. Thus, in the challenging area we have overlapping. According to Figures 9–11, the difference between signal levels in different classes in the proposed smooth sliding digital twin (Figure 9) is much better than in the high-order sliding digital twin (Figure 10) or sliding digital twin (Figure 11) because in this method the signals are much more recognizable in different states (faults) than the other two techniques. Thus, based on these figures, the performance of RMS residual signal classification in the proposed smooth sliding digital twin is better than the other two methods. To test the power of the classification accuracy in the proposed algorithm, the proposed smooth sliding digital twin (proposed algorithm), high-order sliding digital twin, and sliding digital twin are compared. Based on Figure 4, the SVM technique is used for anomaly bearing RMS (indirect) signal diagnosis and crack size identification. In this paper, 25% of the RMS residual signals for the proposed smooth sliding digital twin, high-order sliding digital twin, and sliding digital twin are used for testing, while 75% are used for training. Details about training and testing for crack diagnosis and crack size identification are presented in Table 3.

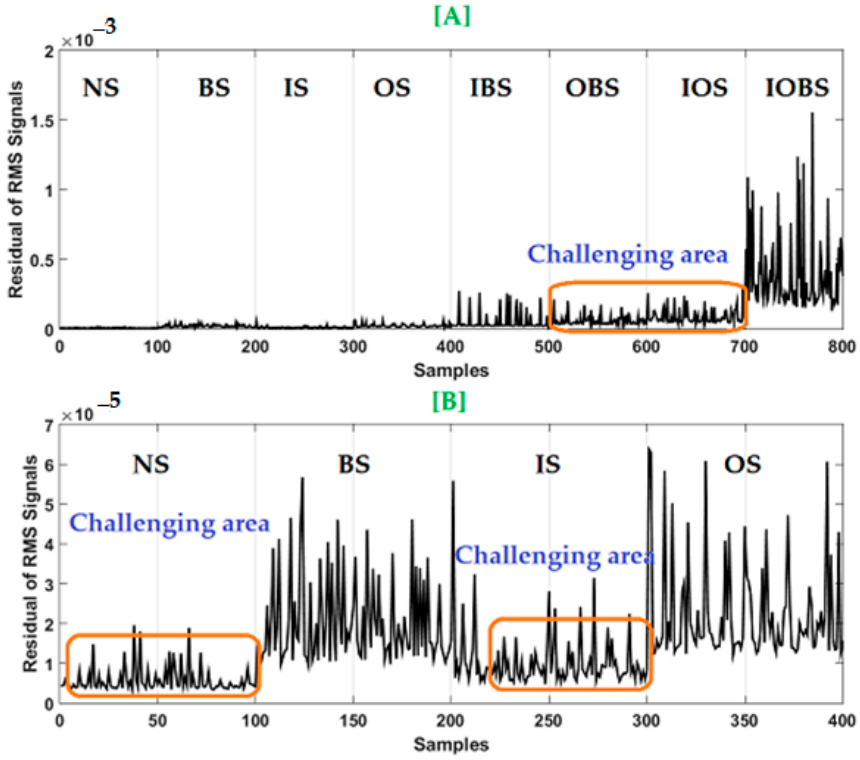

Figure 10. Residual RMS signal using high-order sliding digital twin. (**A**) all conditions, (**B**) zoom view for four conditions.

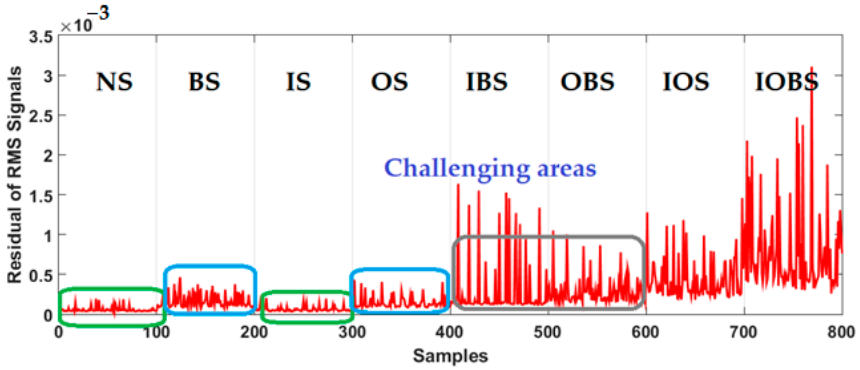

Figure 11. Residual RMS signal using sliding digital twin.

Table 3. The number of samples for training and testing for crack diagnosis and crack size identification.

Conditions	Number of Training (Samples)	Number of Testing (Samples)
Anomaly Diagnosis		
NS	300	100
OS, IS, BS, IOS, IBS, OBS, IOBS	600	200
Crack size identification in the (OS), (IS), (BS), (IOS), (IBS), (OBS), and (IOBS)		
Crack sizes: 3 mm and 6 mm	300	100

Figures 12–14 illustrate the confusion matrices for the combination of the proposed smooth sliding digital twin and SVM, combination of the high-order sliding digital twin and SVM, and combination of the sliding digital twin and SVM.

True Class	NS (%)	BS (%)	IS (%)	OS (%)	IBS (%)	IOS (%)	OBS (%)	IOBS (%)
NS (%)	100	0	0	0	0	0	0	0
BS (%)	0	99	0	0	1	0	0	0
IS (%)	0	0	97	0	2	1	0	0
OS (%)	0	0	0	98	0	2	0	0
IBS (%)	0	0	0	0	96	2	2	0
IOS (%)	0	0	0	0	2	96	2	0
OBS (%)	0	0	0	0	0	2	98	0
IOBS (%)	0	0	0	0	0	0	2	98

Predicted Class

Figure 12. The average of anomaly diagnosis using the combination of proposed smooth sliding digital twin and SVM.

In addition, the averaged accuracy values of anomaly diagnosis based on the combination of the proposed smooth sliding digital twin and SVM, combination of the high-order sliding digital twin and SVM, and combination of the sliding digital twin and SVM are illustrated in Table 4.

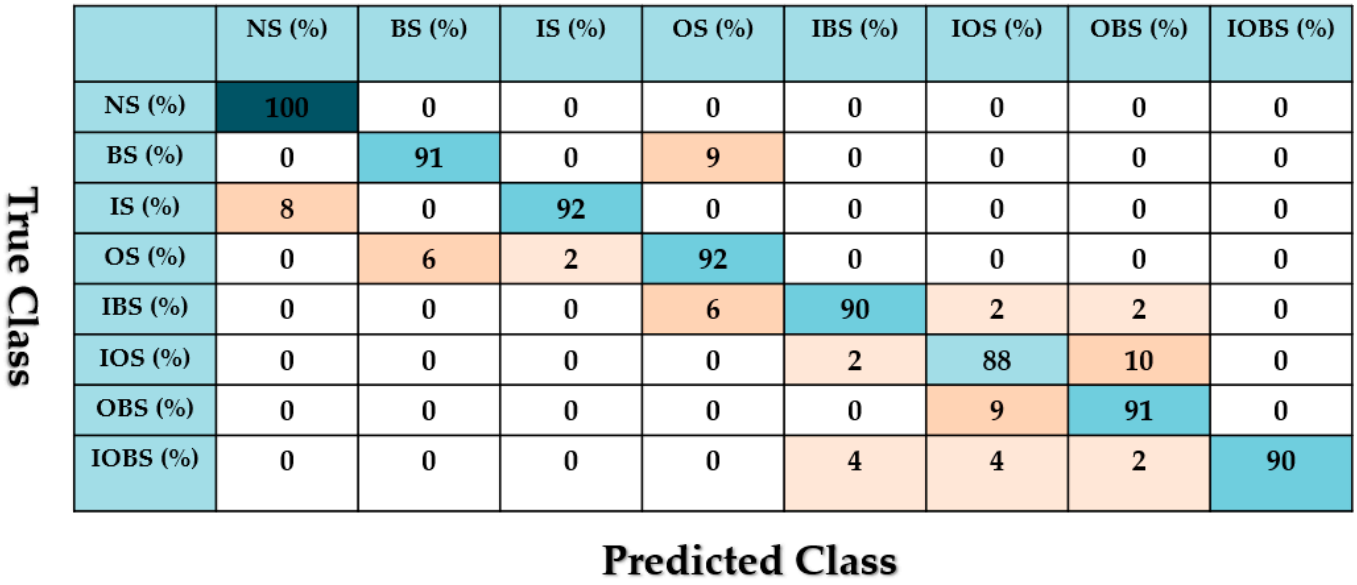

Figure 13. The average of anomaly diagnosis using the combination of high-order sliding digital twin and SVM.

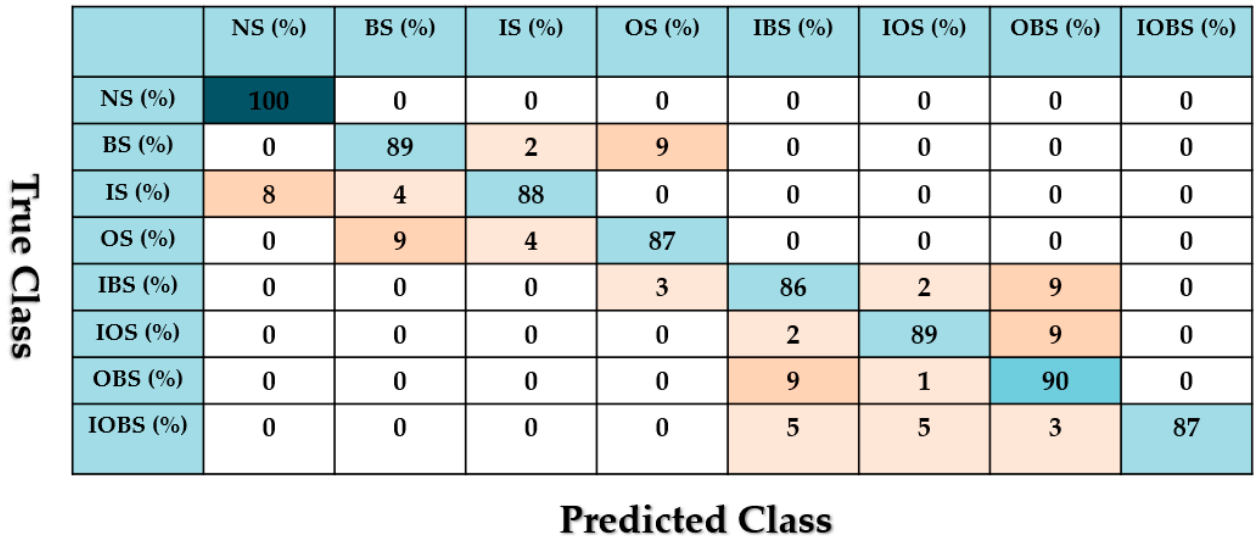

Figure 14. The average of anomaly diagnosis using the combination of sliding digital twin and SVM.

Table 4. Comparison between the combination of the proposed smooth sliding digital twin and SVM, high-order sliding digital twin and SVM, and sliding digital twin and SVM for anomaly diagnosis.

States	Proposed Smooth Sliding Digital Twin and SVM (%)	High-Order Sliding Digital Twin and SVM (%)	Sliding Digital Twin and SVM (%)
NS	100	100	100
BS	99	91	89
IS	97	92	88
OS	98	92	87
IBS	96	90	86
IOS	96	88	89
OBS	98	91	90
IOBS	98	90	87
Average accuracy	97.75	91.75	89.5

Based on these figures and Table 4, when the crack sizes are 3 mm and 6 mm and the motor speeds are 300 RPM, 400 RPM, 450 RPM, and 500 RPM, the average values of the anomaly diagnosis based on the combination of the proposed smooth sliding digital twin and SVM, combination of the high-order sliding digital twin and SVM, and combination of the sliding digital twin and SVM are 97.75%, 91.75%, and 89.5%, respectively. Thus, the anomaly diagnosis performance for the combination of the proposed smooth sliding digital twin is much better than the other two techniques. Based on Figure 13 and Table 4, the critical anomaly diagnosis parts in the combined high-order sliding digital twin and SVM are the IOS and OBS. Moreover, based on Figure 14 and Table 4, the critical anomaly diagnosis parts in the combined sliding digital twin and SVM are the BS, OS, IBS, and OBS.

Furthermore, based on Figure 4, after diagnosis the anomalies, the crack sizes (3 mm or 6 mm) in the BS, IS, OS, IBS, IOS, OBS, and IOBS can be identified using the combination of the proposed smooth sliding digital twin and SVM, combination of the high-order sliding digital twin and SVM, and combination of the sliding digital twin and SVM. This means that the crack size in all (BS, IS, OS, IBS, OBS, IOS, IOBS) conditions is 3 mm or 6 mm. High resolution at this stage leads to more accurate identification of crack size in bearings. Figures 15–21 show the power of the crack size identification using the combination of the proposed smooth sliding digital twin and SVM, combination of the high-order sliding digital twin and SVM, and combination of the sliding digital twin and SVM for the BS, IS, OS, IBS, IOS, OBS, and IOBS conditions, respectively.

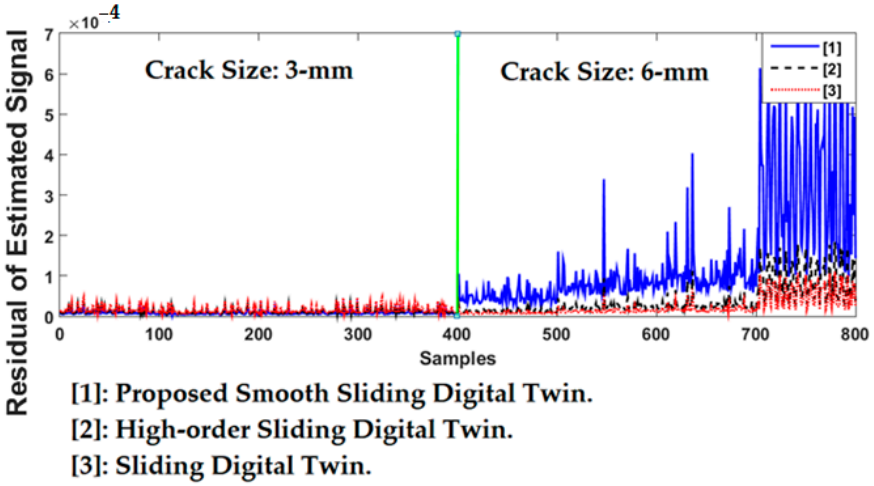

Figure 15. The accuracy of crack size identification for ball residual of RMS signals using proposed smooth sliding digital twin, high-order sliding digital twin, and sliding digital twin.

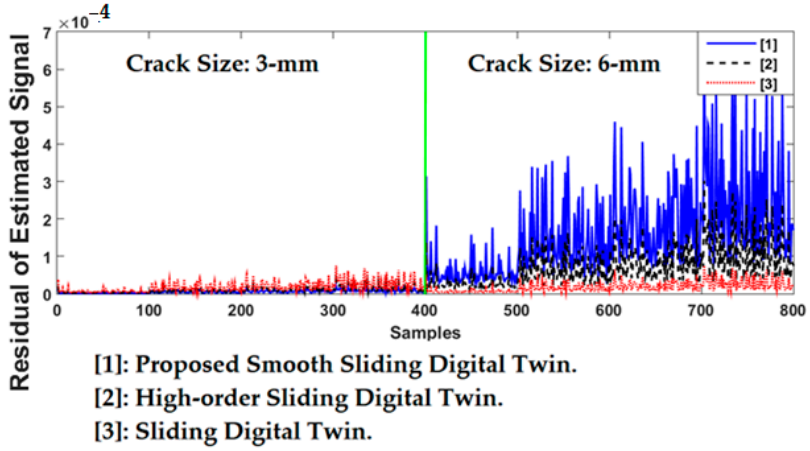

Figure 16. The accuracy of crack size identification for inner residual of RMS signals using proposed smooth sliding digital twin, high-order sliding digital twin, and sliding digital twin.

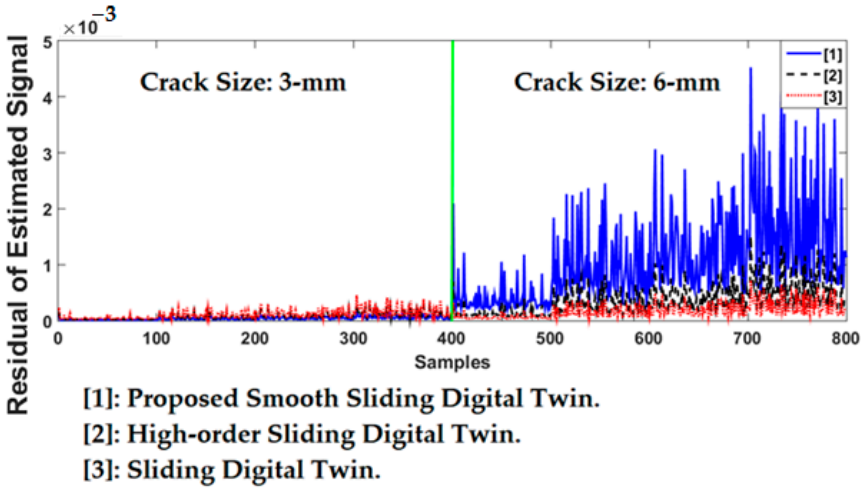

Figure 17. The accuracy of crack size identification for outer residual of RMS signals using proposed smooth sliding digital twin, high-order sliding digital twin, and sliding digital twin.

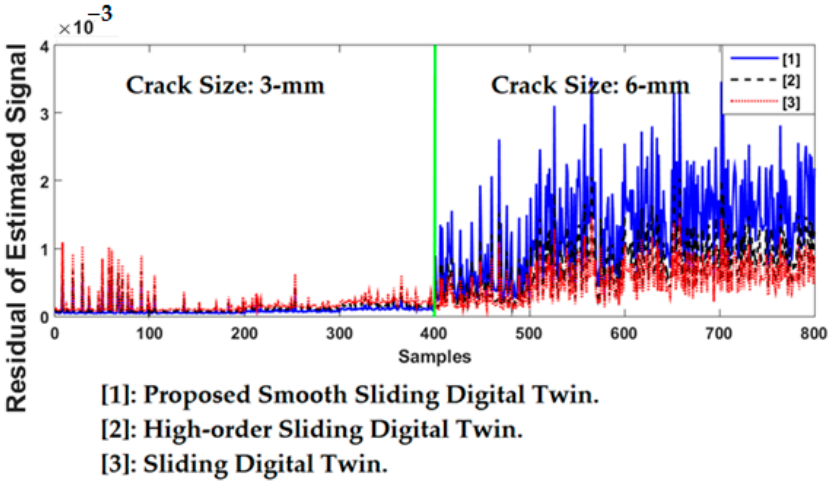

Figure 18. The accuracy of crack size identification for inner-ball residual of RMS signals using proposed smooth sliding digital twin, high-order sliding digital twin, and sliding digital twin.

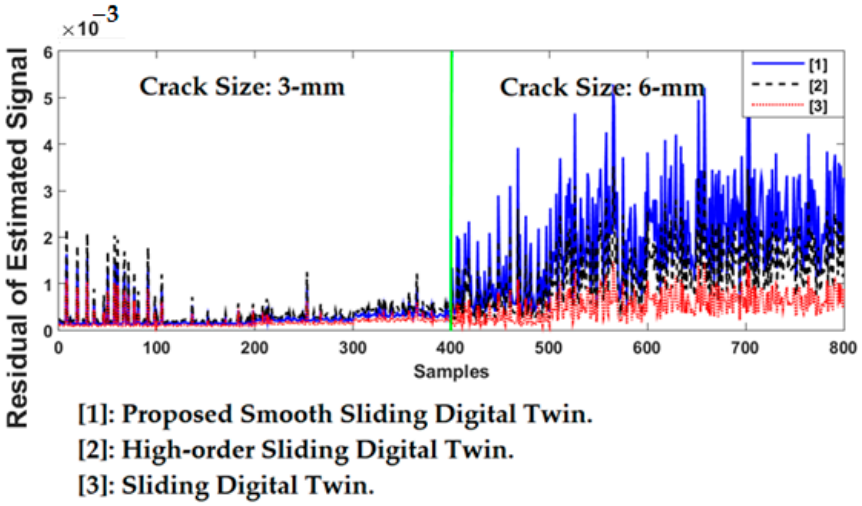

Figure 19. The accuracy of crack size identification for outer-ball residual of RMS signals using proposed smooth sliding digital twin, high-order sliding digital twin, and sliding digital twin.

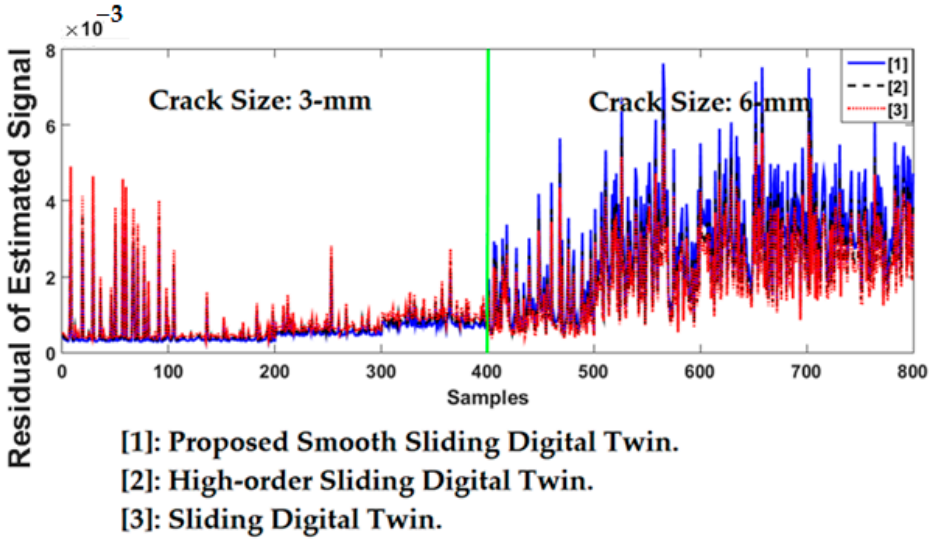

Figure 20. The accuracy of crack size identification for inner-outer residual of RMS signals using proposed smooth sliding digital twin, high-order sliding digital twin, and sliding digital twin.

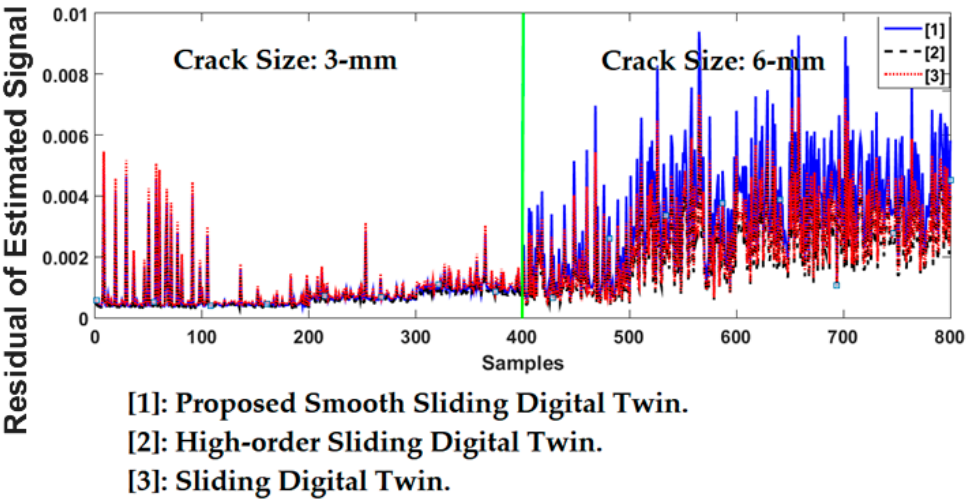

Figure 21. The accuracy of crack size identification for inner-outer-ball residual of RMS signals using proposed smooth sliding digital twin, high-order sliding digital twin, and sliding digital twin.

It can be seen from the figures that in the proposed method in all (BS, IS, OS, IBS, OBS, IOS, and IOBS) faulty conditions, the signal is very separable for 3-mm and 6-mm crack sizes. According to the above figures, the crack size identification performance for the proposed smooth sliding digital twin is better than the other two methods; the power and accuracy of estimation in the proposed smooth sliding digital twin is much better than in the high-order sliding digital twin and sliding digital twin because in the proposed method the signals are much more recognizable for 3 mm and 6 mm in different states (faults) than the other two techniques. Based on Figures 9–11 and 15–21, the proposed smooth sliding digital twin has an excellent performance for fault diagnosis and crack size identification. These figures provide additional evidence that the crack size diagnosis performance is superior in the proposed technique. Furthermore, Table 5 compares the crack size identification accuracies for the combination of the proposed smooth sliding digital twin and SVM, combination of the high-order sliding digital twin and SVM, and combination of the sliding digital twin and SVM.

Table 5. Crack size identification accuracy of the residual RMS signals using the combination of the proposed smooth sliding digital twin and SVM, the combination of the high-order sliding digital twin and SVM, and the combination of the sliding digital twin and SVM.

State	Crack Sizes (mm)	Proposed Smooth Sliding Digital Twin and SVM (%)	High-Order Sliding Digital Twin and SVM (%)	Sliding Digital Twin and SVM (%)
BS	3	98	90	85
	6	98	92	86
IS	3	97	88	86
	6	98	92	88
OS	3	98	90	88
	6	96	91	89
IBS	3	98	89	85
	6	98	92	86
OBS	3	97	90	83
	6	99	93	85
IOS	3	97	90	86
	6	99	91	88
IOBS	3	98	92	85
	6	98	92	86
Average accuracy of size identification		97.78	90.86	86.14

According to the above table, the crack size identification accuracies of the combination of the proposed smooth sliding digital twin approach and SVM, combination of the high-order sliding digital twin and SVM, and combination of the sliding digital twin and SVM are 97.78%, 90.86%, and 86.14%, respectively. Thus, the proposed smooth sliding digital twin has improved the crack size identification accuracy by 6.92 and 11.64 percentage points compared to the high-order sliding digital twin and sliding digital twin, respectively.

Therefore, according to Tables 4 and 5, the accuracy of anomaly diagnosis and crack size classification in the combination of the proposed smooth sliding digital twin and SVM are 97.75% and 97.78%, respectively. These values are 91.75% and 90.86%, respectively, for the combination of the high-order sliding digital twin and SVM and 89.5% and 86.14%, respectively, for the combination of the sliding digital twin and SVM. Thus, based on these two tables, the proposed smooth sliding digital twin has improved the accuracy of anomaly diagnosis and crack size classification by 6 and 6.92 percentage points compared to the high-order sliding digital twin and 8.25 and 11.64 percentage points compared to the sliding digital twin. In the next part, to validate the effectiveness of the proposed smooth sliding digital twin, this approach is compared with following three existing methods including Kalman filter approach [8], classical feedback backstepping observer [9], and variable structure observer [17].

In [8], the authors have used the combination of mathematical-based signal modeling, support vector regression with Laguerre algorithm, and Kalman filter for bearing fault diagnosis. In this approach, the authors used the mathematical approach and identification technique for signal modeling. This approach is complex for modeling and estimation, as well. In addition, in [9], the combination of support vector regression, Gaussian Process Regression, and feedback backstepping observer was suggested for fault diagnosis in the bearing. The main challenge in this approach was stability and robustness. Furthermore, variable structure observer has used for bearing fault diagnosis in [17]. However, the nonlinear autoregression technique was used for system modeling, this technique suffers from high frequency oscillation. To validate the proposed approach further, we calculate the average diagnostic accuracy for (see Table 6) under various operating conditions. Table 6 present the diagnostic accuracy of the proposed smooth sliding digital twin algorithm, Kalman filter (KF) approach [8], classical feedback backstepping (CFB) observer [9], and

variable structure [VS] observer [17] for fault diagnosis in bearing. The diagnostic accuracy is reported as the percentage of correct detection in all data. As shown in Table 6, the proposed smooth sliding digital twin fault diagnosis method outperforms the state-of-the-arts KF observer, CFB observer, and VS technique, yielding average performance improvements of 6.25%, 5.5%, and 6.5%, respectively. This performance improvement can be further validated by the fact that our proposed smooth sliding digital twin method is highly sufficient to identify the fault in the bearing.

Table 6. Comparison between the proposed smooth sliding digital twin, Kalman filter (KF) [8], classical feedback backstepping (CFB) observer [9], and variable structure (VS) observer [17] for anomaly diagnosis.

States	Proposed Smooth Sliding Digital Twin and SVM (%)	KF [8] (%)	CFB [9] (%)	VS [17] (%)
NS	100	100	100	100
BS	99	88	90	91
IS	97	89	88	90
OS	98	89	92	87
IBS	96	90	90	88
IOS	96	92	92	92
OBS	98	90	91	93
IOBS	98	94	95	89
Average accuracy	97.75	91.5	92.25	91.25

5. Conclusions

In this research, a proposed smooth sliding digital twin was used for anomaly diagnosis and crack size identification in bearings based on the AE signals. First, the RMS feature signal was extracted from the AE signals to increase the signal modeling accuracy. Then, the normal RMS feature signal was modeled using the autoregressive fuzzy Gauss–Laguerre approach. This technique is robust and can model the normal RMS signal with high accuracy. Next, a smooth digital twin was proposed for RMS signal estimation in different conditions. This method was designed by combining the proposed modeling algorithm with the proposed estimation scheme. Apart from stability and robustness of the sliding mode digital twin, it has a high-frequency oscillation challenge. To overcome this challenge, a high-order and super-twisting technique was suggested. Furthermore, the fuzzy technique was used with the high-order sliding digital twin to improve the flexibility of signal estimation. Moreover, the combination of the smooth sliding digital twin and SVM was proposed for anomaly diagnosis and crack size identification. The power of the proposed smooth sliding digital twin for anomaly diagnosis and crack size identification was compared with those of the high-order sliding digital twin and sliding digital twin. The proposed smooth sliding digital twin was shown to improve the accuracy of anomaly diagnosis by 6 and 8.25 percentage points compared to the high-order sliding digital twin and sliding digital twin, respectively. Furthermore, the proposed algorithm has enhanced the accuracy of crack size identification by 6.92 and 11.64 percentage points compared to the high-order sliding digital twin and sliding digital twin, respectively. Although the proposed method has a reliable response under unknown conditions, it can be improved in future work by utilizing the parallel combination of the digital twin and deep-learning approach. Moreover, the robust algorithms for modeling and estimation are used to reduce the effect of noise and uncertain conditions. With this combination, the performance of signal estimation and reliability can be improved.

Author Contributions: Conceptualization, F.P., C.-H.K., and J.-M.K.; data curation, F.P.; formal analysis, F.P. and C.-H.K.; funding acquisition, J.-M.K.; methodology, F.P., C.-H.K., and J.-M.K.; software, F.P.; supervision, J.-M.K.; validation, F.P., C.-H.K., and J.-M.K.; visualization, F.P.; writing—original draft, F.P.; writing—review and editing, J.-M.K. All authors have read and agreed to the published version of the manuscript.

Funding: This work was supported by the Technology Development Program (S3126818) funded by the Ministry of SMEs and Startups (MSS, Korea). This work was also supported by a Korea Intelligent Information Society Promotion Agency grant funded by the Ministry of Science and ICT (2022 5G-based Digital Twin Public Leading Project).

Data Availability Statement: The data are available in the UIAI Lab.

Conflicts of Interest: The authors declare no conflict of interest.

References

1. Gundewar, K.S.; Kane, P.V. Condition monitoring and fault diagnosis of induction motor. *J. Vib. Eng. Technol.* **2021**, *9*, 643–674. [CrossRef]
2. Benbouzid, M.; Berghout, T.; Sarma, N.; Djurović, S.; Wu, Y.; Ma, X. Intelligent Condition Monitoring of Wind Power Systems: State of the Art Review. *Energies* **2021**, *14*, 5967. [CrossRef]
3. Liu, Z.; Yang, B.; Wang, X.; Zhang, L. Acoustic Emission Analysis for Wind Turbine Blade Bearing Fault Detection Under Time-Varying Low-Speed and Heavy Blade Load Conditions. *IEEE Trans. Ind. Appl.* **2021**, *57*, 2791–2800. [CrossRef]
4. Grcić, I.; Pandžić, H.; Novosel, D. Fault detection in dc microgrids using short-time fourier transform. *Energies* **2021**, *14*, 277. [CrossRef]
5. Bhat, M.Y.; Dar, A.H. Convolution and correlation theorems for Wigner–Ville distribution associated with the quaternion offset linear canonical transform. *Signal Image Video Processing* **2022**, *21*, 1–8. [CrossRef]
6. Zhao, J.; Hu, T.; Zheng, R.; Ba, P.; Mei, C.; Zhang, Q. Defect recognition in concrete ultrasonic detection based on wavelet packet transform and stochastic configuration networks. *IEEE Access* **2021**, *9*, 9284–9295. [CrossRef]
7. VanDerHorn, E.; Mahadevan, S. Digital Twin: Generalization, characterization and implementation. *Decis. Support Syst.* **2021**, *145*, 113524. [CrossRef]
8. Piltan, F.; Kim, J.M. Bearing anomaly recognition using an intelligent digital twin integrated with machine learning. *Appl. Sci.* **2021**, *11*, 4602. [CrossRef]
9. Piltan, F.; Toma, R.N.; Shon, D.; Im, K.; Choi, H.K.; Yoo, D.S.; Kim, J.M. Strict-Feedback Backstepping Digital Twin and Machine Learning Solution in AE Signals for Bearing Crack Identification. *Sensors* **2022**, *22*, 539. [CrossRef] [PubMed]
10. Ji, S.; Han, B.; Zhang, Z.; Wang, J.; Lu, B.; Yang, J.; Jiang, X. Parallel sparse filtering for intelligent fault diagnosis using acoustic signal processing. *Neurocomputing* **2021**, *462*, 466–477. [CrossRef]
11. TayebiHaghighi, S.; Koo, I. Sensor Fault Diagnosis Using a Machine Fuzzy Lyapunov-Based Computed Ratio Algorithm. *Sensors* **2022**, *22*, 2974. [CrossRef]
12. Xu, Y.; Li, Z.; Wang, S.; Li, W.; Sarkodie-Gyan, T.; Feng, S. A hybrid deep-learning model for fault diagnosis of rolling bearings. *Measurement* **2021**, *169*, 108502. [CrossRef]
13. Allal, A.; Khechekhouche, A. Diagnosis of induction motor faults using the motor current normalized residual harmonic analysis method. *Int. J. Electr. Power Energy Syst.* **2022**, *141*, 108219. [CrossRef]
14. Chen, Y.; Koch, T.; Lim, K.G.; Xu, X.; Zakiyeva, N. A review study of functional autoregressive models with application to energy forecasting. *Wiley Interdiscip. Rev. Comput. Stat.* **2021**, *13*, e1525. [CrossRef]
15. Rahmoune, M.B.; Hafaifa, A.; Kouzou, A.; Chen, X.; Chaibet, A. Gas turbine monitoring using neural network dynamic nonlinear autoregressive with external exogenous input modelling. *Math. Comput. Simul.* **2021**, *179*, 23–47. [CrossRef]
16. Najeh, T.; Lundberg, J. Degradation state prediction of rolling bearings using ARX-Laguerre model and genetic algorithms. *Int. J. Adv. Manuf. Technol.* **2021**, *112*, 1077–1088. [CrossRef]
17. Piltan, F.; Duong, B.P.; Kim, J.M. Deep Learning-Based Adaptive Neural-Fuzzy Structure Scheme for Bearing Fault Pattern Recognition and Crack Size Identification. *Sensors* **2021**, *21*, 2102. [CrossRef]
18. TayebiHaghighi, S.; Koo, I. New Fuzzy Observer Fault Pattern Detection by NARX-Laguerre Model Applied to the Rotating Machine. In Proceedings of the International Conference on Intelligent and Fuzzy Systems, Istanbul, Turkey, 24–26 August 2021; Springer: Cham, Switzerland, 2021; pp. 246–253.
19. Tayebi Haghighi, S.; Koo, I. SVM-based bearing anomaly identification with self-tuning network-fuzzy robust proportional multi integral and smart autoregressive model. *Appl. Sci.* **2021**, *11*, 2784. [CrossRef]
20. Piltan, F.; Kim, J.M. Bearing fault diagnosis using an extended variable structure feedback linearization observer. *Sensors* **2018**, *18*, 4359. [CrossRef]
21. Gao, Z.; Cecati, C.; Ding, S.X. A survey of fault diagnosis and fault-tolerant techniques—Part I: Fault diagnosis with model-based and signal-based approaches. *IEEE Trans. Ind. Electron.* **2015**, *62*, 3757–3767. [CrossRef]

22. Yang, X.; Yao, J.; Deng, W. Output feedback adaptive super-twisting sliding mode control of hydraulic systems with disturbance compensation. *ISA Trans.* **2021**, *109*, 175–185. [CrossRef] [PubMed]
23. Chen, Z.; Wang, X.; Cheng, Y. Adaptive finite-time disturbance observer-based recursive fractional-order sliding mode control of redundantly actuated cable driving parallel robots under disturbances and input saturation. *J. Vib. Control.* **2021**. [CrossRef]
24. Wang, B.; Shao, Y.; Yu, Y.; Dong, Q.; Yun, Z.; Xu, D. High-order terminal sliding-mode observer for chattering suppression and finite-time convergence in sensorless spmsm drives. *IEEE Trans. Power Electron.* **2021**, *36*, 11910–11920. [CrossRef]
25. Appana, D.K.; Prosvirin, A.; Kim, J.-M. Reliable fault diagnosis of bearings with varying rotational speeds using envelope spectrum and convolution neural networks. *Soft Comput.* **2018**, *22*, 6719–6729. [CrossRef]
26. Md Junayed, H.; Manjurul Islam, M.M.; Kim, J.-M. Acoustic spectral imaging and transfer learning for reliable bearing fault diagnosis under variable speed conditions. *Measurement* **2019**, *138*, 620–631.
27. Islam, M.M.M.; Kim, J.-M. Time–frequency envelope analysis-based sub-band selection and probabilistic support vector machines for multi-fault diagnosis of low-speed bearings. *J. Ambient. Intell. Humaniz. Comput.* **2017**, 1–16. [CrossRef]